Theor Chem Acc (2007) 117:885–901
DOI 10.1007/s00214-006-0209-y

REGULAR ARTICLE

Structure and dynamics of mesogens using intermolecular potentials derived from *ab initio* calculations

Claudio Amovilli · Ivo Cacelli · Giorgio Cinacchi · Luca De Gaetani · Giacomo Prampolini · Alessandro Tani

Received: 16 June 2006 / Accepted: 13 October 2006 / Published online: 19 December 2006

Abstract A method for the calculation of the two-body intermolecular potential which can be applied to large molecules is presented. Each monomer is fragmented in a number of moieties whose interaction energies are used to recover the interaction energy of the whole dimer. For these reasons this strategy has been called fragmentation reconstruction method (FRM). By a judicious choice of the fragmentation scheme it is shown that very accurate interaction energies can be obtained. The sampling of the potential energy surface of a dimer is then used to obtain intermolecular force fields at several levels of complexity, suitable to be employed in bulk phase computer simulations. Applications are presented for benzene and for some mesogenic molecules which constitute the principal interest of the authors. A number of properties ranging from phase stability, thermodynamic quantities, orientational order parameter and collective dynamics properties are computed and discussed.

Keywords Condensed matter · Simulation methods · Liquid crystals · ab initio force field

1 Introduction

In the theoretical approach to material science and, in particular, to liquid crystal (LC) field, computer simulations methods such as Monte Carlo (MC) and molecular dynamics (MD) are by far the most employed [1–4]. The structural and dynamic macroscopic properties, obtained through simulations, are derived from the adoption of a model potential, which contains the description of the molecular framework and interactions. The strong dependence of LC phase stability from the molecular features [1,5,6] makes the understanding of the link between microscopic structure and macroscopic mesophase properties a challenge for the scientific community. This extraordinary sensitivity to the details of the molecular structure arises [2,6] from a complex interplay between energetic effects (as the molecular interactions: electrostatic, dispersive and inductive forces) and entropic ones (like positional, orientational and conformational distributions). From a thermodynamic point of view, the balance among these free energy terms is critical for the (meso-)phase stability. Small variations in the molecular framework can alter this delicate equilibrium, affecting significantly the phase diagram of the system.

As a matter of fact, it is in the force-field (FF) specification that the microscopic interactions are introduced in the simulation method, and the chemical identity of the molecule finds a correspondence in the bulk observables. In particular, in LC field the abovementioned delicate interplay between the forces governing the mesogenic properties calls for very specific molecular models. This poses some doubts on the reliability of a straightforward adoption of the most widely employed FF's [7–10], since their extension to large LC forming molecules, can be done only invoking a high degree of transferability. Indeed, it has been pointed out that small differences in the molecular structure may produce impressive variations in the macroscopic properties, so that transferability must be used with caution.

C. Amovilli · I. Cacelli (✉) · G. Cinacchi · L. De Gaetani · G. Prampolini · A. Tani
Dipartimento di Chimica e Chimica Industriale,
Università di Pisa, via Risorgimento 35,
56126 Pisa, Italy
e-mail: ivo@dcci.unipi.it

In principle, the Car–Parrinello method [11,12] has the potentiality of solving the problem. However, its actual implementation appears problematic for systems where dispersion forces are dominant and its application to large molecular systems and long-time dynamics remains a future objective. The same reasons rule out a direct application of the *ab initio* Born–Oppenheimer molecular dynamics to mesogenic molecules.

In this context, we have recently [13–16] proposed a scheme which couples first principle calculations with bulk simulations. The idea of constructing new FF's from first principle calculations was developed in consideration of the necessity of improving the efficiency of the literature FF's, which usually rely on some experimental data, to mimic mesogenic properties in experimental conditions. This *ab initio* approach is based on modeling the FF on the base of a number of quantum mechanical (QM) calculations, performed on a set of representative intermolecular geometries. Owing to the high computational request of accurate QM calculations, this alternative scheme has been rarely used [17–23], although it presents several advantages. First, these *ab initio* derived (ABD) FF's are suited to the chosen molecule and take into account its chemical identity: no degree of transferability must be invoked for such interaction potentials. Moreover, the *ab initio* computed potential energy surface (PES) constitutes a reference database for parameterization of model potentials of different complexity. This possibility appears to be of particular importance for LC's, as it allows one to tune the "realism" of the model on the set of properties that should be reproduced. In some cases, e.g., where a full atomic (FA) representation is computationally too expensive, simplified models are to be used [3,15,24–28]. Finally, since ABD FF's are not driven by experimental data, simulation models can be constructed even for molecules whose properties are difficult to measure, giving in principle predictive capabilities to the whole approach.

The major drawback of this route of parameterization is that the *ab initio* calculation of accurate intermolecular energies of dimers, through standard QM techniques, becomes quickly unfeasible when the molecular dimensions increase. To circumvent the problem, we have proposed the fragmentation–reconstruction method (FRM) [13,14] which allows us to accurately compute the interaction PES of dimers of large molecules, making use of *ab initio* calculations. The basic idea behind FRM is that many large molecules can be thought of as composed of a rather small number of moieties, e.g., phenyl rings and hydrocarbon chains, which contribute separately to the two body molecular interaction energy. The smaller size (and possibly higher symmetry) of the latter fragments makes them amenable to accurate *ab initio* calculations at a reasonable computational cost.

A rational scheme to implement the FRM for the study of condensed phase properties can be summarized as follows.

1. FRM: calculation of intermolecular (and intramolecular) potentials with quantum mechanical methods
2. Fitting: parameterization of the computed energies through model potential functions suitable for computer simulations
3. Simulation: MD or MC simulations and comparison of the resulting macroscopic properties with the relevant experimental data

This scheme was tested for a selected group of molecules of increasing complexity. In the present work, results for benzene [29,30], p-*n*-oligophenyls (nPh) series [15,26,28] and 4-*n*-alkyl, 4′ cyano-biphenyl (nCB) series [13,14,16,31–33] will be reported. The benzene molecule was chosen since its dimer constitutes a demanding test for *ab initio* calculations of the interaction energy and has been extensively studied from a theoretical point of view [10,17–19,34–41]. Moreover, a realistic model with full atomic detail can be handled in computer simulations and it is actually necessary if one wants to quantitatively reproduce benzene macroscopic properties. The FRM approach has been then applied to the two homologues series nPh and nCB. nPh's offer unique advantages as their structure is very simple, with just one type of fragment (the phenyl ring) and basically a single kind of internal coordinate, the torsional inter ring dihedral. The higher members of the series are able to form mesophases, such as a nematic phase for the *p*-quinquephenyl and even a smectic phase for the six ring member. The nCB series is a classical benchmark for LC theoretical studies [42–52], both for its simplicity and for the abundance of experimental data [45,53–63]. Longer chain members present a fairly rich polymorphism at room temperature, with smectic (for $n \geq 8$) as well as nematic phases (for $n \geq 5$). For these properties nCB's find direct applications in material science like thin films and liquid crystal displays [64,65].

The paper is organized as follows. In Sect. 2 we discuss the FRM and the model potentials employed in computer simulations. Section 3 contains the main computational details on QM, MC and MD calculations. In Sect. 4 the main applications are collected, and the results for selected test-case molecules are reported and compared with the relevant experimental data.

2 Methods

2.1 Fragmentation–reconstruction method

For the calculations of the interaction potential of large molecules, through the use of standard QM programs, we have developed the FRM [13,14] by resorting to an old suggestion of Claverie [66], who proposed approximating the interaction energy as a sum of atom–atom interactions. Our approach relies on the assumption that the interaction energy of a dimer can be approximated to a good accuracy as a sum of energy contributions between each pairs of fragments into which the two molecules can be decomposed. The basic criterion behind this fragmentation scheme is that the ground state electronic density around the atoms of each fragment has to be as close as possible to that around the same atoms in the whole molecule. The main advantage of this approach lies in the possibility of performing calculations between moieties much smaller than the whole molecules under study. This allows us to include electronic correlation effects and to obtain a good estimate of the dispersion energy which is expected to account for a large fraction of the attractive intermolecular energy for most of the molecules that can form mesophases. The informations gained about the interaction energy between the fragments pairs are then used to set up the full intermolecular energy.

The first step of the FRM approach is a decomposition of the whole molecule into fragments by cutting properly chosen single bonds. The valence of the resulting fragments is then saturated by suitable "intruder" atoms or small groups. This allows us to express the intermolecular energy as a sum of contributions of all resulting pair of fragments. Obviously, the intruder groups have to be subsequently canceled from the molecule and their energy contributions properly subtracted in order to recover the total interaction energy between the two original molecules.

By way of example, let's consider the cyano-biphenyl (0CB) molecule CN–C_6H_4–C_6H_5. The 0CB molecule may be split into cyano-phenyl and benzene fragments through a cut along the ring-ring bond and then saturated with hydrogen atoms. Thus the whole molecule can be formally written as

$$CNC_6H_4\text{–}C_6H_5 = CNC_6H_4\text{–}H_a + H_b\text{–}C_6H_5 - H_b\text{–}H_a$$

where the two intruder atoms H_a and H_b are first included to saturate the resulting fragments and then removed as a H_a–H_b molecule. It is worth noticing, as shown in Fig. 1, that the spatial position of the fragments is unchanged with respect to the whole molecule and that the location of the "intruder" atoms H_a and H_b is unambiguously determined by the internal geometry of the saturated fragments. In the 0CB case, this results in a slightly altered bond distance of the "intruder" H_2 molecule (0.68 Å, instead of the equilibrium value of 0.74 Å). This fragmentation path can be summarized by

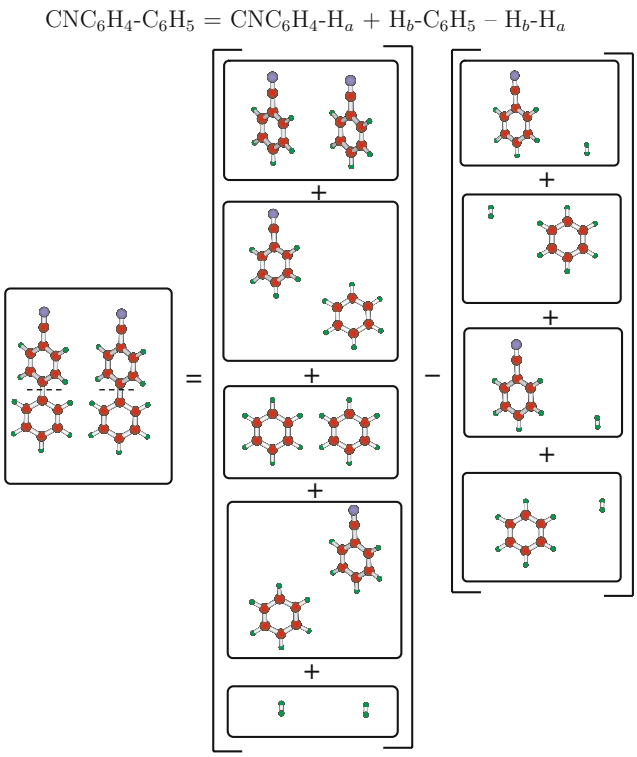

Fig. 1 Application of the FRM scheme to the 0CB dimer. The interaction energy of the 0CB dimer in a chosen configuration (*left side*) is computed as a sum of the fragment-fragment contributions, as shown on the *right side*. The broken bond is shown on the left with a *dashed line*

$$0CB = CB + B - H_2,$$

where CB=cyano-phenyl and B=benzene, and leads to the following expression for the total FRM interaction energy of the dimer

$$\begin{aligned} E^{\mathrm{FRM}}_{0CB-0CB} = {} & E_{CB-CB} + E_{B-B} + E_{CB-B} + E_{B-CB} \\ & + E_{H_2-H_2} - E_{CB-H_2} - E_{H_2-CB} \\ & - E_{B-H_2} - E_{H_2-B}. \end{aligned}$$

Here, E_{X-Y} (X, Y = CB, B, H_2) is the computed interaction energy between fragment X of the first 0CB molecule and fragment Y of the second. It can be easily verified that, if N is the number of electrons of the 0CB, the above expression correctly includes N^2 interactions for intermolecular energy. This method was successively reproposed by Zhang et al. [67], who applied it to study interactions between molecules of biological interest.

2.2 Model intermolecular potentials

The FRM PES, $E^{\mathrm{FRM}}(\mathbf{R}, \mathbf{\Omega})$, is sampled for a large number of dimer conformations, identified by the distance $\mathbf{R}$ between the molecular centers of mass and the three Euler angles $\mathbf{\Omega}$. The resulting energy database is then fitted onto a model potential function $U(\mathbf{R}, \mathbf{\Omega})$ suitable for computer simulations. The parameters $\mathbf{P}$ of the intermolecular functions, that characterize the chosen model, are obtained from a least square fitting procedure, by the minimization of the functional

$$I = \frac{\sum_{k=1}^{N_{\mathrm{geom}}} w_k \left(E_k^{\mathrm{FRM}} - U_k[\mathbf{P}]\right)^2}{\sum_{k=1}^{N_{\mathrm{geom}}} w_k} \tag{1}$$

where N_{geom} is the number of geometries considered, w_k an appropriate weight at the geometry $k \equiv [\mathbf{R}, \mathbf{\Omega}]$.

The choice of the functional form of $U(\mathbf{R}, \mathbf{\Omega})$ is driven by a compromise between model accuracy and computational convenience. In the last few years, many models of different complexity have been employed by our group [14,15,26,28–30]. In the present work we report in some detail only the results achieved with two kinds of models, namely the nGBQ model [15,28] and the FA model [14,16,30,31]. The former is a coarse grained model which groups all the atoms of a phenyl ring into a single interaction site, represented with an oblate Gay–Berne ellipsoid [68,69] plus a linear quadrupole [70] perpendicular to the phenyl plane. The FA model represents an accurate potential for computer simulations and is obtained by considering each atom of the molecule as an interacting site. This atomistic model can be often simplified by assembling together groups of atoms (e.g., methyl or methylene) into single interaction sites. The atomistic FA model potential, adopted to fit the FRM energies of a dimer A $\cdots$ B, can be expressed as a sum of site-site contributions:

$$U^{\mathrm{FA}}(\mathbf{R}, \mathbf{\Omega}) = \sum_i^{N_A} \sum_j^{N_B} u_{ij}(\mathbf{R}, \mathbf{\Omega}) \tag{2}$$

where N_A and N_B are the number of interaction sites of molecule A and B respectively, while u_{ij} is the intermolecular energy contribution of sites i and j. The site-site function is a modified form of the 12-6 Lennard–Jones (LJ) potential, plus the standard electrostatic interaction, namely

$$u_{ij} = 4\epsilon_{ij}\left[\left(\frac{\xi_{ij}\sigma_{ij}}{r_{ij} + \sigma_{ij}(\xi_{ij} - 1)}\right)^{12} - \left(\frac{\xi_{ij}\sigma_{ij}}{r_{ij} + \sigma_{ij}(\xi_{ij} - 1)}\right)^{6}\right] + \frac{q_i q_j}{r_{ij}} \tag{3}$$

The parameter ξ is introduced in the LJ contribution, to allow the well width to vary independently from its depth and position, thus improving the model flexibility and, in particular, its ability of representing correctly the shape of the low energy repulsive branch.

Finally, although not attempted in this work, one can think of different site-site potential forms for dispersion energy. For example, a new semi-empirical interaction potential for nanostructured graphitic systems has been recently developed in our laboratory [71] by resorting to a special π-electron network model. Similar applications may be considered in future studies for materials which include such graphitic structures.

2.3 Molecular flexibility

A major advantage achieved by increasing the level of complexity from single site to multi site models is the possibility of taking molecular flexibility into account. In MC and MD simulations this is usually done by assuming the energy as the sum of two decoupled contributions, namely inter- and intra-molecular terms, i.e.,

$$E(\mathbf{r}_A, \mathbf{r}_B; \mathbf{R}, \mathbf{\Omega}) = E^{\mathrm{inter}}(\mathbf{r}_A, \mathbf{r}_B; \mathbf{R}, \mathbf{\Omega},) + E^{\mathrm{intra}}(\mathbf{r}_A) + E^{\mathrm{intra}}(\mathbf{r}_B) \tag{4}$$

where $\mathbf{r}_A$ and $\mathbf{r}_B$ collect the internal coordinates of molecules A and B, respectively. The adopted intramolecular potential has the AMBER [9] form

$$E^{\mathrm{intra}} = E^{\mathrm{stretch}} + E^{\mathrm{bend}} + E^{\mathrm{tors}} + E^{\mathrm{LJintra}} \tag{5}$$

where the terms in the sum have the expressions:

$$E^{\mathrm{stretch}} = \sum_i^{N_{\mathrm{bonds}}} k_i^s \left(r_i - r_i^0\right)^2; \; E^{\mathrm{bend}} = \sum_i^{N_{\mathrm{angles}}} k_i^b \left(\theta_i - \theta_i^0\right)^2$$

$$E^{\mathrm{tors}} = \sum_i^{N_{\mathrm{dihedrals}}} \sum_{j=1}^{N\cos_i} k_{ij}^d [1 + \cos(n_j^i \delta_i - \gamma_j^i)];$$

$$E^{\mathrm{LJintra}} = \sum_i^{N_{\mathrm{LJintra}}} \sum_{j=i+4, i+5, \ldots} u_{ij}^{\mathrm{LJ}}$$

where u_{ij}^{LJ} has the form of the standard LJ potential.

The set of parameters describing the intramolecular part of the potential can be taken from literature FF data [7–9] or re-parameterized with the aid of single molecule QM calculations. In the following, the intramolecular parameters have been taken from the AMBER force-field, except for those involving internal coordinates of particular importance in determining the overall molecular shape as, for instance, the core-chain dihedral angle in nCB.

3 Computational details

3.1 FRM calculations

In view of the very large number of geometries to be considered for the computation of the interaction energy of all pairs arising from the fragmentation scheme, a reasonable compromise between accuracy and computational cost has to be found. In order to properly consider the dispersion energy, we have chosen the Möller–Plesset second order perturbation theory (MP2) in the supermolecule approach. Methods like extensive implementations of the configuration interaction or coupled cluster with perturbative corrections have been discarded because considered too expensive for the present scope. On the other hand, no reliable DFT functional has been yet found for Van der Waals interactions. All energies were computed using the counterpoise correction scheme, to take care of the basis set superposition energy error (BSSE) [72]. Up to date, although often questioned, this is accepted as the standard correction [73] for the incompleteness of the basis set. The employed basis set is the standard 6-31G* basis set modified for the low exponent of the d Gaussian Type Orbitals centered on the Carbon and Nitrogen atoms: $\alpha_d = 0.25$ versus usual values of 0.7-0.9, as originally proposed by Hobza et al. [37].

The geometry of each molecule in the dimer was taken frozen in all binding energy calculations. The optimization of the monomer geometry was performed by the well tested density functional B3LYP method [74] with triple-zeta basis set 6-311G(2d,p). The obtained geometries were practically coincident with the experimental ones and no appreciable differences in the binding energy of the dimer was noticed [13,14,16,30] by using the theoretical or the experimental geometry.

All QM calculations were performed with the Gaussian package [75].

3.2 Computer simulations

Monte Carlo runs have been performed according to the usual rules of the NPT scheme, using a code written in our group. During the runs a molecule was selected at random and trial displacements of its center of mass and inertia axes were performed. In order to sample the intramolecular conformational space, the relevant internal coordinates were also modified according to the Metropolis [76] scheme. Finally, the shape and the volume of the computational box were changed during simulations, by attempting to vary a randomly selected edge of the box.

Molecular dynamics simulations were performed with the parallel version of the Moscito3.9 package [77], modified to take the ξ parameter into account. Unless differently stated, all runs were performed in the NPT ensemble, with P = 1 atm and different temperatures. Temperature and pressure were kept constant using the weak coupling scheme of Berendsen et al. [78]. In all cases, the bond lengths were kept fixed at their equilibrium value using the SHAKE algorithm [79] and a timestep of 1–1.5 fs was used. Electrostatic long range interactions were treated with the particle mesh Ewald method [80,81], using a convergence parameter α of 5.36 and a 4^{th} order spline interpolation. The short range intermolecular interactions have been truncated at $R_c = 11$ Å and $R_c = 10$ Å for benzene and nCB, respectively. Standard corrections for energy and virial [82] were employed in all simulations.

4 Applications

4.1 A test case: benzene

The *ab initio* calculation of the benzene dimer interaction energies is a challenging task. Since the sum of electrostatic and induction forces is in general repulsive and the formation of the Van der Waals complexes is due to dispersion interaction, the MP2 method seems adequate since it accounts for a large part of the correlation energy [13,29,30]. The reliability of the results, obtained in a relatively cheap way, is demonstrated in Fig. 2 through a comparison with the results of Tsuzuki et al. [40], which are probably the most accurate in the literature. The geometries corresponding to energy minima are close to each other and the order of the energies is correctly reproduced. It is worth mentioning that for aromatic molecules, the use of MP2 with large basis set, can lead to a large overestimate of the binding energy [36]. Nevertheless, the agreement between these results and the best literature data confirm that the basis set used in this work is sufficient to detect with a good precision the most stable configurations and that the basic intermolecular interactions are correctly included in the resulting potential.

The FA model, hereafter referred as ABD potential, has been fitted onto the PES database, sampled with $\simeq 200$ geometries. The parameters have been obtained with the fitting procedure described by equation (1) and are reported in Reference [30].

The calculation of the second virial coefficient

$$B_2(T) = -\frac{N_A}{2}\int \mathrm{d}\mathbf{r}\int \mathrm{d}\mathbf{\Omega}\left[\mathrm{e}^{-U^{\mathrm{inter}}(\mathbf{r},\mathbf{\Omega})/k_BT} - 1\right]$$

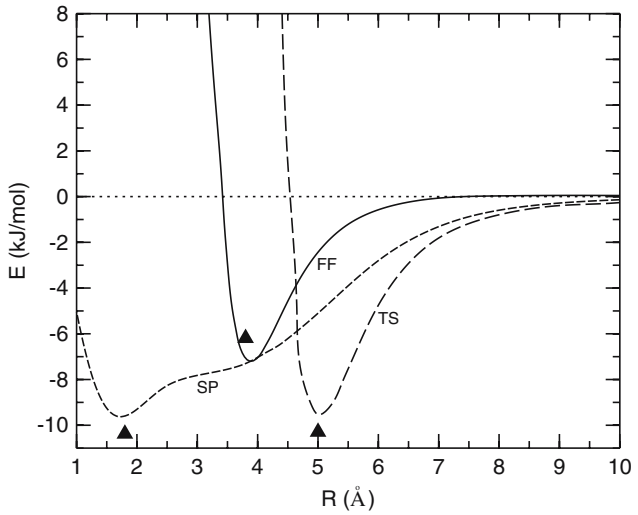

Fig. 2 Interpolated curves of *ab initio* interaction energies, computed for the benzene dimer in face to face (*FF*), T-shaped (*TS*) and slipped parallel (*SP*) arrangements. In the *TS* geometry one hydrogen of a molecule points towards the center of the other molecule. The distance between the benzene planes in the *SP* configuration is 3.3 Å. The results of reference [40] are reported with full triangles

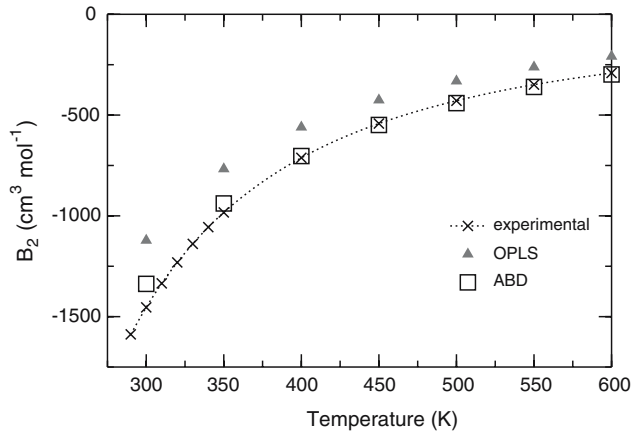

Fig. 3 Benzene second virial coefficient versus temperature. Comparison between experimental [83,84] (*dotted line* and *crosses*) and theoretical results obtained by OPLS [10] (*full triangles*) and ABD [30] (*empty squares*) potentials

constitutes a first test on the quality of the ABD potential. In Fig. 3, our results are compared with experimental data [83,84] and with that derived from literature OPLS potential [10]. Both models seem able to reproduce the main features of the benzene-benzene interaction to a good level of accuracy. Above T = 400 K, the ABD potential is in quantitative accord with experimental results, while small deviations occur at lower temperatures. Both the overall quality of the *ab initio* calculations and the accuracy of the fitting are confirmed by these results. Considering its nature as an effective two-body potential [10] a worse performance of the OPLS was to be expected for a strictly two-body property like B_2.

To take into account internal degrees of freedom, the intermolecular ABD [30] and OPLS [10] were coupled with the same intramolecular part, whose expression is given in Eq. 5. The resulting FF's will be labeled **A** and **J**, respectively. Parameters describing the intramolecular energy were also reported in detail in Reference [30].

Simulations at 1 atm, in the 138–350 K range of temperatures, were performed with both **A** and **J** FF's on a system of 400 molecules, initially placed in the experimental geometry of the benzene crystal lattice [85]. Two different condensed phase were characterized, namely a crystal and an isotropic liquid phase. In Fig. 4 the averaged values of the enthalpy and the density are reported as a function of the simulation temperature, while several thermodynamic properties are compared with the relevant experimental data in Table 1. As expected, the **J** model well reproduces both experimental density and enthalpy of vaporization, i.e., properties exploited for OPLS [10] parameterization. It is worth noticing that the **A** system melts at a temperature closer to the experimental one, though the melting enthalpy is underestimated. Indeed, the initial ordered phase was stable up to 340 K with the **J** FF and to 310 K with the **A** one, with runs of 0.5 and 1.5 ns, respectively. In particular, the crystalline structure of model **J** remains stable at 320 K for more than 4 ns. Cell parameters, density and intermolecular energy for the crystals are also reported in Table 1, while more details on characterization of benzene liquid structure can be found in the source paper [30]. In conclusion, the performance of the ABD potential on the thermodynamic and structural properties well compares with the OPLS [10] which has been constructed on the base of some of such properties.

For any FF, a reliable validation must include dynamic properties. To this end, NVE runs were performed on liquid structures previously equilibrated in the NPT ensemble at room temperature. In the study of rotational diffusion, rigid molecules were used for computational convenience. As can be seen from Table 2, the translational diffusion is slightly underestimated by all models. For OPLS model this seems to be a known deficiency, already found by other authors [41], whereas the **A** results are closer to the experimental values. The parallel and perpendicular rotational diffusion coefficients show that both rigid models describe the reorientation of the C_6 axis much the same way, and compare fairly well with the experiment. On the contrary, rotation about the C_6 seems to be overestimated by model **A**.

Table 1 Benzene experimental and calculated thermodynamic properties. Densities ρ refer to the crystal (218 K) and liquid (300 K) phases. Intermolecular energy (U) and cell parameters (a, b, c) refer to the crystalline structure at 218 K. α and c_p are the thermal expansion coefficient and the heat capacity of the liquid 300 K, determined respectively from the slope of the density and enthalpy curves, reported in Fig. 4 for the two models

	Units	Exp	Model **J**	Model **A**
ρ (218 K)	g/cm^3	1.055 [85]	1.060 ±0.002	1.055 ±0.005
U (218 K)	kJ/mol	–45.1 [86]	–44.9 ±0.12	–45.4 ±0.18
a (218 K)	Å	7.44 [85]	7.24	7.38
b (218 K)	Å	9.55 [85]	9.51	9.35
c (218 K)	Å	6.92 [85]	7.09	7.10
T^{melt}	K	278.64 [87]	340 ±10	310 ± 5
ΔH^{melt}	kJ/mol	9.3 [87]	8.4 ± 0.8	6.6 ± 0.6
ρ (300 K)	g/cm^3	0.874 [84]	0.893 ± 0.003	0.911 ± 0.005
α (300 K)	10^{-3} g cm^{-3} K^{-1}	1.198 [88]	1.35 ± 0.005	1.14 ± 0.007
c_p (300 K)	J/mol K^{-1}	135.69 [89]	64 ± 9	83 ± 8
ΔH^{vap}	kJ/mol	33.92 [90]	34.9 ± 0.23	36.9 ± 0.25

Table 2 Experimental [41,91] and calculated translational (D) and rotational ($\Theta_\parallel, \Theta_\perp$) diffusion coefficients for benzene

Model	T (K)	ρ(g/cm^3)	D (10^{-5}cm^2/s)	$\Theta_\parallel$ (10^{10}rad^2/s)	$\Theta_\perp$ (10^{10}rad^2/s)
J	300	0.885	1.7	23.0	12.5
A	300	0.902	2.1	35.0	12.4
exp	298	0.874	2.27	15.9–28.8	7.4–10.2

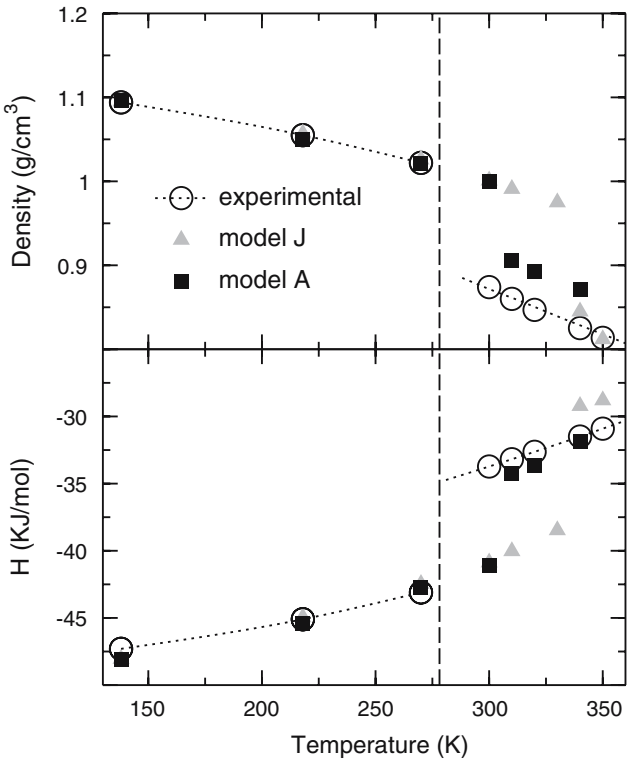

Fig. 4 Enthalpy H and density as a function of temperature for **J** and **A** benzene FF's. *Dashed vertical line* indicates the experimental melting temperature (278.6 K)

Finally, benzene collective dynamics has been studied calculating the various viscosities according to the well known Green-Kubo relations. By looking at Table 3, both models appear to reproduce satisfactorily the experimental shear viscosity (η_S) at $\simeq$ 300 K. Although measurements of bulk viscosity (η_B) are more scarce, a recent study of acoustic relaxation time [93] reports that η_B should not exceed 0.36 η_S, which is closer to the results of model **A**. The latter also seems to qualitatively account for the temperature dependence of viscosity.

4.2 FRM tests

Once the reliability of the intermolecular energy for the benzene dimer has been demonstrated, the FRM scheme has been applied to the series of *p*-phenyls [15, 26,28], with a number of phenyl rings from two to five. The *p*-phenyls are fragmented in a number of benzene molecules by operating cuts along ring-ring σ bonds. The biphenyl molecule is amenable for direct MP2 calculations whose results can be used to test the validity of the FRM approach. This comparison is reported in Fig. 5 for the face to face dimer conformation. It is apparent that the reconstruction approach does not alter the characteristic features of the dimer PES and the differences are lower than the uncertainties of both set of values.

A further test was performed [14] on the dimer of 0CB, the smaller homologue of the nCB series. In this case we have also checked the capability of the FRM to reproduce the effect of the dihedral conformation on the two body interaction energy. The reconstruction test was carried out for three different PES's sections, each characterized by a fixed value of the ring-ring torsional angle

Table 3 Benzene experimental [92] and calculated shear (η_S) and bulk (η_B) viscosities

model	T(K)	η_S (cP)	η_B (cP)
J	277	0.79 ± 0.080	0.49 ± 0.044
A	278	0.84 ± 0.024	0.39 ± 0.066
exp [92]	283	0.76	–
J	303	0.58	0.41
A	301	0.57 ± 0.024	0.18 ± 0.002
exp [92]	303	0.56	–
A	328	0.46 ± 0.020	0.24 ± 0.03

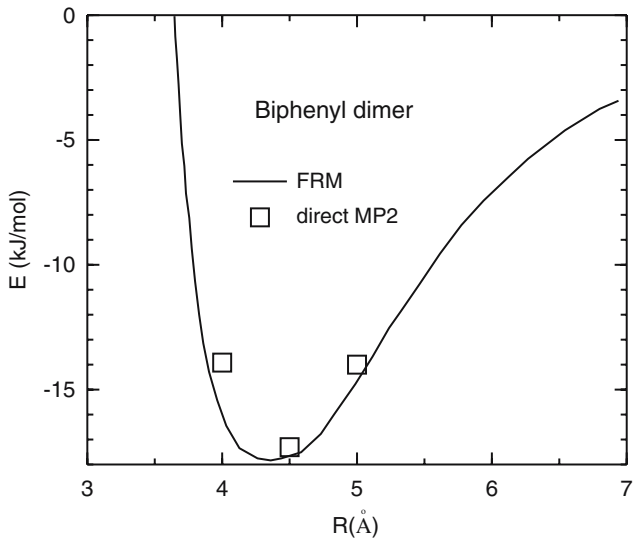

Fig. 5 Energy curve of the biphenyl dimer for the face to face configuration. The angle between the two rings is kept fixed at 42°. FRM curve (*solid line*) and direct *ab initio* MP2 data (*empty squares*) are reported

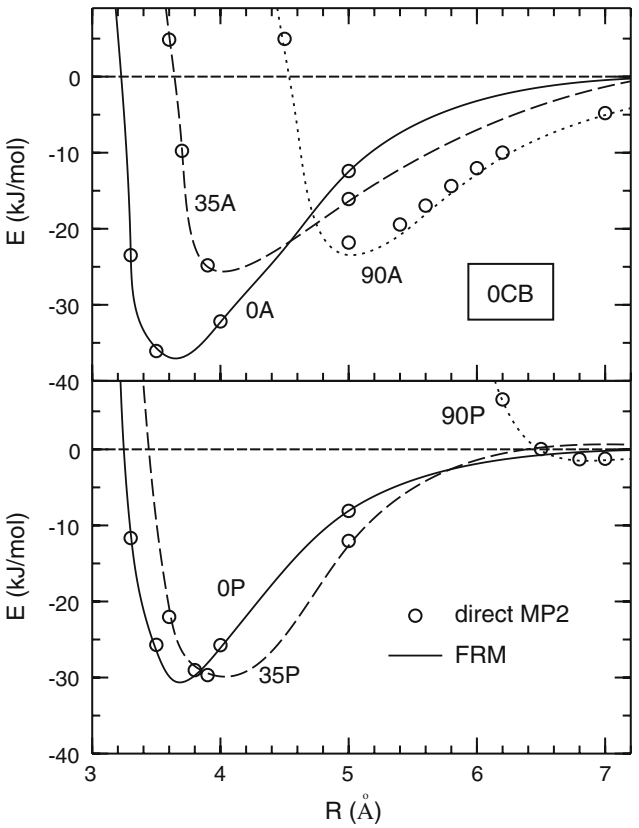

Fig. 6 Direct MP2 and FRM energies for antiparallel (*upper panel*) and parallel (*lower panel*) arrangements of the 0CB dimer. In both figures, directly computed *ab initio* MP2 energies are reported with *empty circles*, while FRM curves are shown with *solid*, *dashed* and *dotted lines* for $\phi = 0°, 35°$ and 90°, respectively

ϕ in both molecules. By fixing ϕ at 0° (planar conformation), 35° and 90°, in the parallel (**P**) and antiparallel (**A**) geometries, we obtain six arrangements, namely 0**P**, 35**P**, 90**P** and 0**A**, 35**A**, 90**A**. The computed energies for all these sets are reported in Fig. 6.

It is apparent that the agreement between the direct MP2 calculations and the reconstructed FRM data is satisfactory, since the MP2 curves are well reproduced. The absolute maximum difference amounts to 0.7 kJ/mol for the parallel arrangements (0**P** at $\mathbf{R} = 3.3$ Å) and raises to 1.7 kJ/mol for the antiparallel conformations (90**A** at $\mathbf{R} = 5.0$ Å). Comparison between data computed for different dihedral values provides a further critical test of the accuracy of the FRM. Since it cannot take into account inter ring conjugation, the reliability of FRM is expected to be more delicate when the two rings are coplanar. By the data of Fig. 6, it is evident that such a problem does not arise, at least for neutral molecules, where the contributions of quinoid structures are expected to be negligible.

In conclusion, the above tests support our confidence that intermolecular potentials can be obtained via FRM with basically the same accuracy as for direct *ab initio* calculations. Moreover large molecules, which are not amenable to standard QM methods, may become accessible by using FRM. Finally, FRM calculations require much less CPU time than the standard direct procedure.

4.3 *p-n*-phenyls

The PES of the five-ring member of the nPh series, calculated through FRM, is shown in Fig. 7 for selected

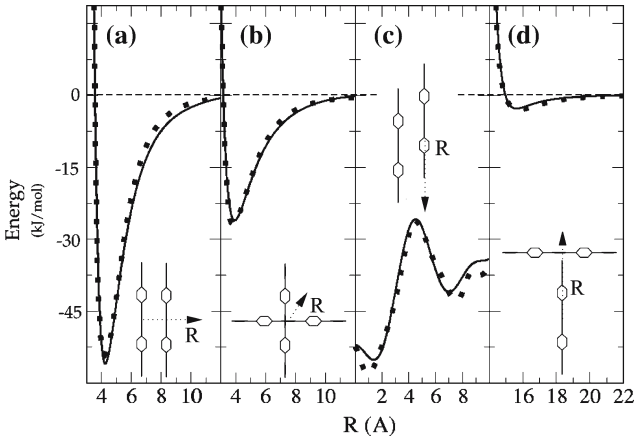

Fig. 7 Fitted FRM curves for different arrangements of p-quinquephenyl: **a** parallel sandwich; **b** cross; **c** parallel displaced; **d** T-shaped. FRM and nGBQ energies are reported with *dots* and *solid lines*, respectively

configurations. Similar results have been obtained for the other members of the series. As expected from simple considerations, the interaction energy increases significantly along the series for the parallel configurations, while it is almost constant for T-shaped, cross and end-to-end configurations. This trend suggests that the increasing shape anisotropy, i.e., the elongation of the rod-like molecule, results in an augmented tendency of the dimer to prefer aligned conformations, presumably favoring orientationally ordered bulk phases. In particular, a displacement along the long axis direction allows the molecules to reach stable configurations, making the parallel displaced geometries as stable as the parallel sandwich ones.

The hybrid, multi-site nGBQ model constitutes a coarse grained level in our hierarchy of models, lying between single site models and fully atomistic pair potentials. As can be seen from Fig. 7, the nGBQ model is capable of accurately describing the FRM PES. From the parallel displaced configuration curve, it can be noted for instance the effect of the quadrupolar interaction which shifts the minimum towards the slipped configuration, in reasonable agreement with the quantum mechanical results. The intermolecular nGBQ potential has been coupled [28] to an intramolecular torsional potential that drives the ring-ring flexibility. The latter was previously derived from accurate single molecule DFT calculations [94]. The resulting coarse grained FF has been employed in NPT-MC simulations.

The equilibration of MC runs has been assessed by monitoring the evolution of a number of observables such as enthalpy, density and orientational order parameter, P_2. The latter quantity may range from 1 (completely aligned crystalline sample) to 0 (perfectly isotropic liquid), assuming values between 0.7 and 0.4 in a typical nematic phase. We have simulated systems of 600 molecules at atmospheric pressure and several temperatures. The equilibration runs were started from the simple cubic crystal structure, with dihedral angles between two contiguous discs set to the value of $\sim 45°$, which corresponds to the minimum of the torsional energy as calculated in [94].

Some of the results are compared with experimental data in Table 4. The melting points (T_m) were determined in simulation by considering the average value between the highest temperature in the solid and the lowest in the liquid phase for each oligophenyl; clearing (T_{NI}) and boiling (T_b) points where determined analogously. In this way the computed values are affected by a ± 25 K uncertainty. The range of stability of the phases is reproduced by the simulation, although the transition enthalpies are underestimated, with relative deviations increasing along the series. For p-quinquephenyl, at T = 675 K we have obtained a value of the orientational order parameter of ~ 0.5 in the experimental temperature range (660–688 K) of the nematic phase [95].

Of particular importance for the oligophenyls series is the dependence of the dihedral angles between two contiguous rings on the thermodynamically stable phase at a given temperature. In the biphenyl molecule, for instance, the angle between the two rings is around 40° in gas phase [97,98], 32° in liquid phase [99], while the molecule is found in a nearly planar conformation in crystalline phase [100]. A similar behavior is also found for the other members of the series [101]. As shown in Fig. 8, a neat change in population can be observed for all members at the transition between crystalline and liquid phase and the experimental trend is well reproduced.

In conclusion the nGBQ model, despite its simplicity, describes at a semi-quantitative level the phase diagram of the *p*-oligophenyl series, and turns out to be useful in modeling very large molecules, where the computational costs do not allow more detailed models. Moreover, the comparison of the results with those of single site GB models [15,26] has shown the importance of molecular flexibility on the resulting bulk properties.

4.4 5CB

The fragmentation of the 5CB molecule ($CN–C_6H_4–C_6H_4–C_5H_{11}$) was performed by a very natural choice of the fragments:

$$CN–C_6H_4–H_a(BCN);\ H_b–C_6H_4–H_c(B);\ H_d–C_5H_{11}(P)$$

where two C–C single bonds in the 5CB are substituted by C–H bonds in the isolated fragments. This partition retains the closed shell nature of the aromatic rings as

Table 4 Thermodynamic results of the nGBQ model for *p*-n-phenyls

n		T_m	T_{NI}	T_b	ΔH_m	ΔH_{NI}	ΔH°_{vap}
2	calc	375	–	575	14.2	–	27.4
	exp	344 [a]	–	529 [b]	18.8 [a]	–	54.0 [b]
3	calc	425	–	725	17.1	–	34.6
	exp	493 [a]	–	658 [b]	35.4 [a]	–	79.0 [b]
4	calc	575	–	825	17.7	–	56.7
	exp	587 [a]	–	773 [b]	37.8 [a]	–	117.0 [b]
5	calc	625	675	875	11.4	7.9	65.1
	exp	660 [a]	688 [a]	823 [b]	42.3 [a]	0.9 [a]	151.0 [b]

Temperatures are in K and ΔH's are in kJ/mol. Experimental data: [a]Ref. [95] [b]Ref. [96] and references therein

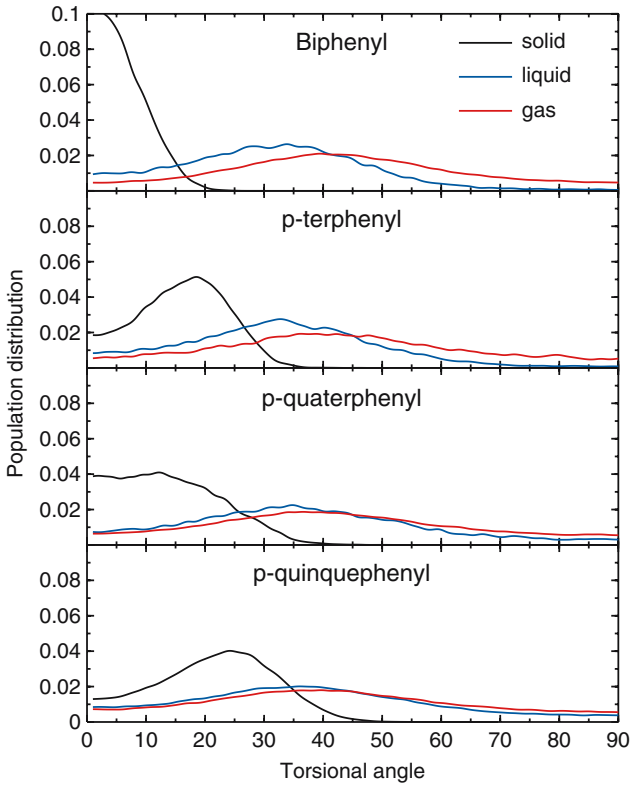

Fig. 8 Population distribution of the first torsional angle (degrees) along the *p*-oligophenyls series. For all molecules, distributions in solid, liquid and gas phases are reported with *black*, *blue* and *red lines*, respectively

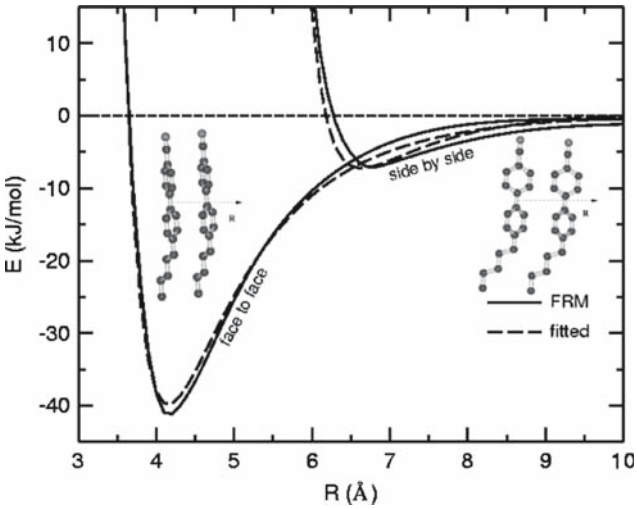

Fig. 9 FRM (*solid line*) and fitted FA model (*dashed line*) energy curves for the 5CB dimer. The face to face and side by side arrangements are considered

well as of the aliphatic chain and makes possible to compute accurate intermolecular energies between the three saturated fragments.

The FRM PES was fitted [14] with a FA potential suitable for computer simulations. In this model, the methyl and methylene groups of the chain are both considered as a single site, thus dropping out all the aliphatic hydrogen atoms. On the contrary, all aromatic hydrogens were explicity considered. Some constraints were imposed to the fitting parameters in order to take into account equivalent sites and, in particular, to gain transferability to longer homologues: the three inner methylene groups were treated as equivalent sites with $q_{CH_2} = 0$. The resulting parameters are given in Reference [14], together with some details of the fitting procedure.

Some sections of the resulting FA PES are compared in Fig. 9 with the corresponding FRM curves. The agreement for all the considered configurations is good. The face to face geometries were obtained by translating the second 5CB molecule along the normal to the plane of the cyano-phenyl ring. This dimer energy presents a local minimum of -40 kJ/mol at about 4.2 Å, the main source of attractive contributions arising from the interactions between the aromatic rings. When the translation vector lies perpendicular to both the normal to the cyano-phenyl ring and the 5CB long axis (side by side arrangements), the resulting curve has a shallow energy minimum at much higher distances. A similar accuracy was reached in all the considered geometries [14], being the fitting standard deviation less than 2.5 kJ/mol.

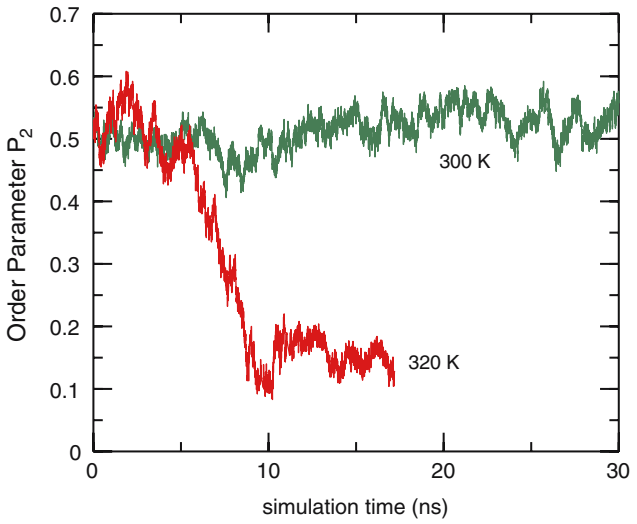

Fig. 10 The order parameter P_2 of the 5CB system is reported as a function of the simulation time for two different runs at 300 and and 320 K

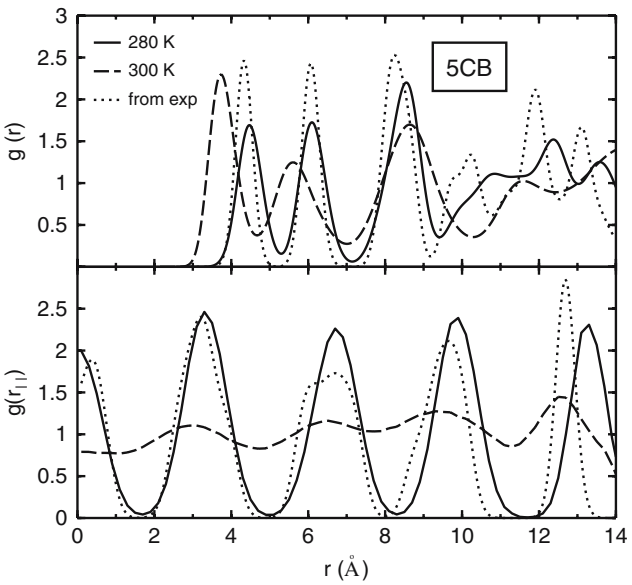

Fig. 11 Pair correlation functions of the 5CB crystal. Experiment derived [16,55] (*dotted line*), and MD results at T = 280 K (*solid line*) and at T = 300 K (*dashed line*) are reported. In the bottom panel the $g(r_{\|})$ shows the loss of positional order along the director at 300 K

The intramolecular part of the 5CB FF was constructed [16] adopting AMBER [9] parameters for the transferable internal degrees of freedom (as bending angles or aromatic ring dihedrals) and by deriving those more specific (as the core-chain dihedral or the inter-ring angle) from single molecule DFT calculations.

The starting configuration for MD simulations of the crystal was set by placing four molecules per unit cell with the experimental geometry [55] at 253 K. This unit cell was replicated 4, 3, 4 times along the x, y, z direction, respectively, obtaining in such a way a system of 192 molecules.

In order to find the range of stability of the crystal, four runs at different temperatures, namely 200, 250, 280 and 300 K, were performed at atmospheric pressure The lattice was stable up to 300 K, where it underwent a phase transition. When the system was heated at this temperature the positional order along the director was lost in less than 2 ns, and the system started the melting process to a more disordered phase (see lower panel of Fig. 11). The residual orientational order was removed by heating the system until complete isotropy was reached. From this trajectory, partially ordered configurations were extracted as starting points for the runs in both nematic and isotropic phases. Five different runs were performed at 290, 300, 310, 320 and 330 K. The equilibration was assessed by looking at three different quantities, namely the internal energy, the bulk density and the order parameter, P_2. As can be seen in Fig. 10, P_2 as a function of time indicates a phase transition from an ordered phase to an isotropic liquid in the 300–320 K temperature range. The ordered phase has also been recognized as nematic through the study of the pair correlation functions [16].

As regards the crystal phase, the cell parameters (a, b and c), the density (ρ) and the equilibration time (τ) are reported in Table 5 together with the experimental values [55]. At 280 K, the system was equilibrated for 13.5 ns and the computed pair correlation functions are reported in Fig. 11 together with those derived from the experimental [55] X-ray diffraction crystal data (see Reference [16] for details). No major difference results, being the simulated structure in good agreement with the experimental function at short range, despite an overestimation of the crystal density of about 5%.

Concerning internal geometries, the crystal phase is characterized by a enhanced population of the *gauche* conformation of the first dihedral in the aliphatic chain ($\simeq$ 90% at 280 K). In the nematic phase the chain tends to be more elongated (all *trans* conformation) towards rodlike geometry, while in the liquid no preferential arrangement is observed [16]. The average dihedral angle between the two phenyl rings is $\simeq 25°$ in the crystal and increases to more than 30° in the nematic and isotropic phases. It is worth noticing that this increase is not a simple consequence of the augmented temperature, but it is strongly related to the packing effects in the crystal lattice. These findings correctly reproduce the experimental behavior [55,56].

To assess the stability of the nematic phase, and to verify the ergodicity of the simulations, three different

Table 5 Calculated and experimental [55] crystal data at several temperatures

T (K)	τ (ns)	ρ(g/cm^3)	a (Å)	b (Å)	c (Å)
200	1.5	1.229 ± 0.0013	8.26	15.39	10.58
250	1.5	1.207 ± 0.0016	8.33	15.44	10.65
280	13.5	1.194 ± 0.0021	8.38	15.45	10.69
253 [55]	–	1.15	8.25	16.02	10.93

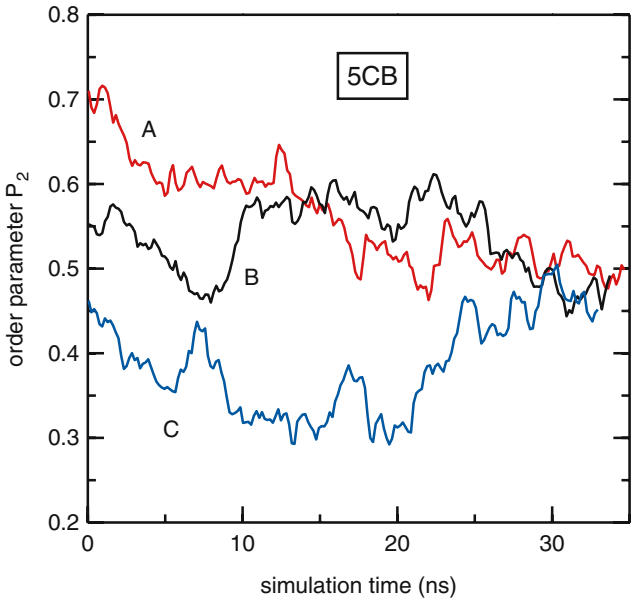

Fig. 12 Three MD runs starting from 5CB configurations at different P_2 value (run A: 0.75; run B: 0.52; run C: 0.43) and identical thermodynamic conditions

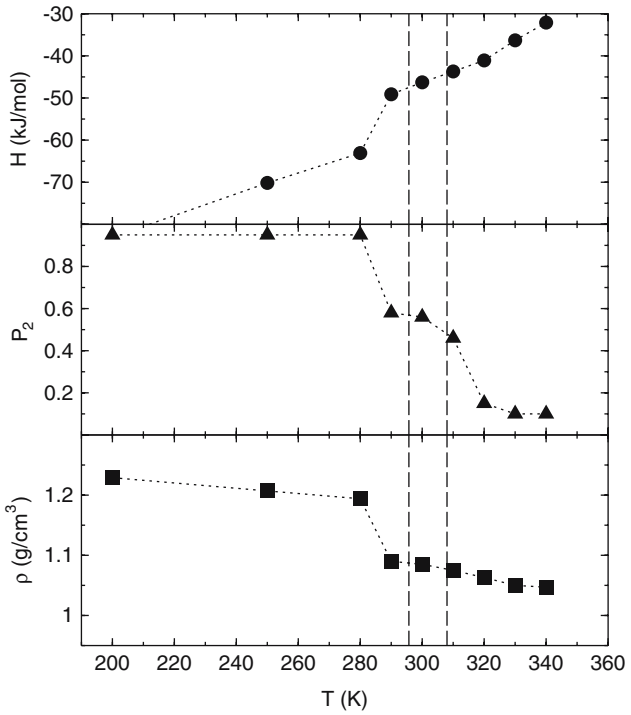

Fig. 13 Average thermodynamic properties as a function of temperature for 5CB. The dotted vertical line indicate the experimental [58] transition temperatures

starting structures were created, namely 0.75 (run A), 0.52 (run B) and 0.43 (run C), each with a different degree of orientational order but equal values of pressure and temperature. This kind of study was previously attempted [102] for a similar molecule, but no convergence to an unique value of P_2 was observed. Thanks to the increase of computational resources, very long simulations were performed in Reference [16], allowing in this way the three runs to eventually reach a common value of orientational order, as reported in Fig. 12. Even though free energy calculations would be a safer proof of true thermodynamic equilibrium, this test seems to indicate a stable nematic phase at 290 K. It is noteworthy to point out that in run C a spontaneous reordering can be observed.

Average density, order parameter and enthalpy of the equilibrated systems, reported in Fig. 13, were calculated as a function of temperature. The thermal expansion coefficient (α) was calculated from the slope of the density versus temperature curve, while the melting enthalpies (ΔH^m and ΔH^c) were estimated from the jumps (melting and clearing, respectively) of the enthalpy curve (see Fig. 13). These thermodynamic properties are compared with their experimental value in Table 6 at 300 and 320 K. The density of the proposed model is overestimated for all explored temperatures. Minor differences result for ΔH^m and ΔH^c. Most important, the phase transitions of the system are at temperatures very close to the experimental ones.

Table 6 Experimental and calculated thermodynamic properties for 5CB

	Units	Exp	This work
ρ (300 K)	g/cm^3	1.020 [57]	1.085 ± 0.03
ρ (320 K)	g/cm^3	0.995 [57]	1.063 ± 0.04
α	10^{-3} g cm^{-3}	0.7 [57]	1.3
T_m	K	287.72 [58]	295 ± 5
T_c	K	306.7 [58]	315 ± 5
ΔH^m	kJ/mol	15.95 [58]	11.4 ± 0.7
ΔH^c	kJ/mol	0.54 [58]	-1.0 ± 1.0

Table 7 Computed (D_k) and experimental [103] (D_k^{exp}) translational diffusion coefficients in nematic and isotropic phase of 5CB

T (K)	D_k ($\times 10^{-10} m^2/s$)	D_k^{exp} ($\times 10^{-10} m^2/s$)
300 (k = ∥)	0.49	0.66
300 (k = ⊥)	0.21	0.27
300 (k = iso)	0.28	0.37
315 (k = iso)	0.63	0.69

5CB dynamic observables can be grouped into two broad classes, short time and long time properties. Our results [31] of translational diffusion coefficients (a short time property) are compared with experimental values in Table 7. The activation energy estimated from all values, including D_{iso} of the nematic phase ($D_{iso} = D_{\parallel}^{\frac{1}{3}} D_{\perp}^{\frac{2}{3}}$) is 32.3 ± 5 kJ/mol, in very good agreement with the experimental result 32.8 ± 0.5 kJ/mol [103]. Although this accord might well be fortuitous, it's certainly rewarding as activation energies are considered among the most reliable experimental data. On the contrary, as regards rotational diffusion, experimental data of the perpendicular coefficient $D_{\perp}^{rot}$ in nematic bulk phases seem to suffer of some uncertainty [104,105], so that they are often biased by some model approximation [59] or assumed [106,107]. Furthermore, the 5CB literature values of $D_{\parallel}^{rot}$, range from 0.5 to 3.5 $\cdot 10^9 s^{-1}$ [59,106,107]. The latter well agree with our of $1.4 \times 10^9 s^{-1}$ and $2.2 \times 10^9 s^{-1}$ at 290 and 300 K, respectively. Considering this good accord on the parallel coefficient, MD simulations may be considered an additional technique to possibly overcome the indeterminacy of $D_{\perp}^{rot}$.

The 5CB's rheo-dielectric behavior has been studied by monitoring the long axis reorientation as well as the viscosities in the bulk. As both these collective dynamic properties are typically long time processes, the simulations were extended as long as possible ($\simeq$ 10 ns in the isotropic phase and $\geq$ 15 ns in the nematic) to improve the statistical accuracy. From the upper panel of Fig. 14, where the reorientational correlation function F(t) is reported, it is evident that the relaxation process occurs on the ns time scale. The marked difference in the relaxation times τ_R, associated with the decay of F(t), can be attributed to the effect of the nematic mean field, which constraints the molecular long axis to tumble around a preferred orientation aligned with the director.

As can be seen from the data reported in Table 8, the agreement between experimental [63] and computed shear viscosities is very good at all temperatures. From these values, following Landau-deGennes (LdG) theory [6], the relaxation time τ_{LdG}, that is related to the randomization process of the pseudo-nematic domains

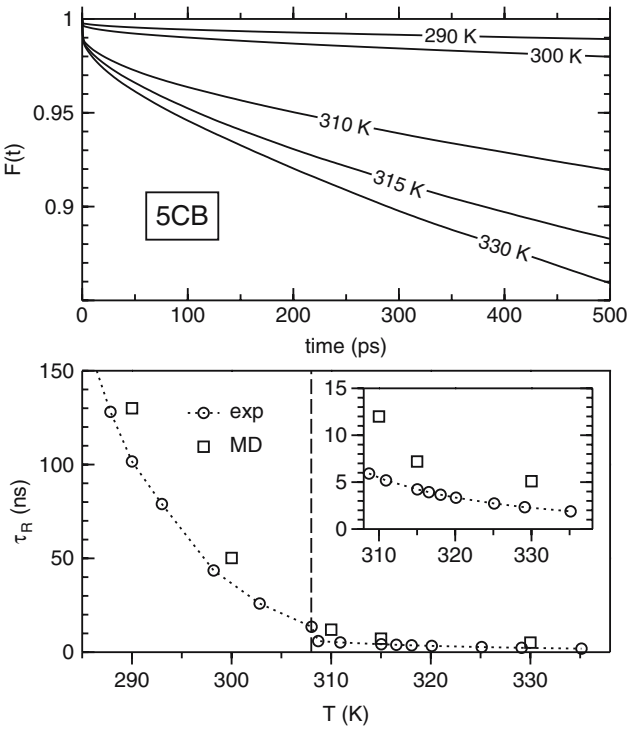

Fig. 14 Dielectric relaxation functions F(t) and dielectric relaxation times τ_R. In the upper panel the computed functions F(t) are shown for the nematic (T = 290 K, T = 300 K) and the isotropic (T= 310, 315 and 330 K) phases, respectively. In the lower panel, the experimental [60,61] (*circles*) and the computed (*squares*) τ_R are reported as a function of temperature. The temperature dependence in the isotropic phase is highlighted in the inset on the right side

Table 8 Computed and experimental [63,108] values of long time properties in the isotropic phase of 5CB. From left to right: shear (η_S) viscosity, longitudinal viscosity (η_L) Landau-deGennes relaxation times τ_{LdG}

T (K)	η_S (mPa s)	η_L (mPa s)	η_S^{exp} (mPa s)	τ_{LdG} (ns)	τ_{LdG}^{exp} (ns)
310	25.4	94	23.8	144	139
315	22.2	75	19.0	63	49
330	12.0	33	11.0	11	9

[6,109], can be computed as

$$\tau_{\mathrm{LdG}} = \frac{V_{\mathrm{eff}}^{*}\, \eta_S(T)}{k_B(T - T^{*})}$$

where V_{eff}^{*} has been taken as the simulation box volume divided by the number of molecules, k_B is the Boltzmann constant and we have used for T^* the nematic to isotropic transition temperature ($T_{NI} = 305$ K). The agreement between computed τ_{LdG} values and experimental optical Kerr effect results ($\tau_{\mathrm{LdG}}^{exp}$, [108]) derives

from the aforementioned good description of viscosity, assuming a similar estimate of the effective molecular volume $V^*_{\rm eff}$.

This satisfactory agreement is encouraging since indicates that the proposed method, which include no a posteriori information (except the crystalline structure), can really have predictive capabilities.

4.5 nCB

In the FA model employed for 5CB, the methylene CH_2 groups are treated as single interaction sites and considered as equivalent (i.e., they are endowed with identical intermolecular parameters) and neutral ($q_{CH_2} = 0$). This allows us to easily extend the 5CB intermolecular potential to higher homologues (namely 6CB, 7CB and 8CB) by simply adding a methylene site to the aliphatic chain. Even the intramolecular potential already used for 5CB can be extended with no effort to the nCB series, retaining the parameters adopted to describe bending and torsion in the aliphatic chain.

Preliminary runs were performed on 6CB, 7CB and 8CB, and similar behavior of thermodynamic quantities upon temperature was found [32] in the series. The clearing temperatures from an orientationally ordered phase to an isotropic liquid were estimated through very long runs (> 35 ns for each temperature) and reported together with experimental values in Fig. 15 as a function of the number of carbon atoms in the chain. The well known [110–113] odd-even effect is well reproduced. Upon heating, from an initial crystalline configuration, the 8CB system shows an highly orientationally ordered phase ($P_2 > 0.6$). Preliminary analysis, as reported in Fig. 16, showed a layered structure along one direction, indicating the presence of a smectic structure. If confirmed, the appearance of such mesophase, in accord with the experimental findings, would be another proof of the quality of the proposed potential.

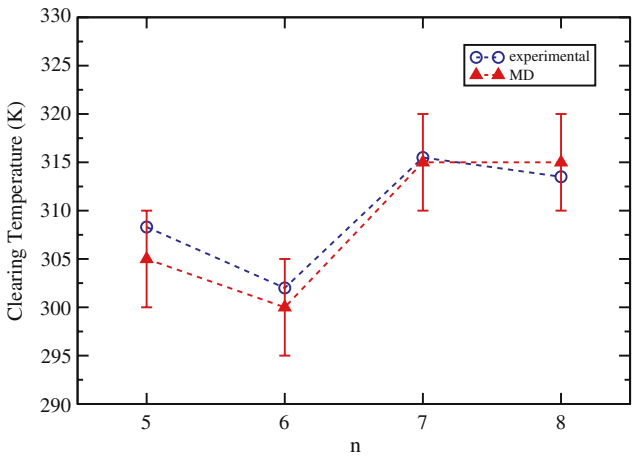

Fig. 15 Odd-even effect in the nematic to isotropic transition temperatures in the nCB series

5 Conclusions

We have outlined in this paper a new approach to the computational study of condensed phase systems, composed of fairly complex molecules. As many mesogenic molecules can be decomposed into a few building blocks (e.g. phenyl rings and aliphatic chains) the FRM appears ideally suited to obtain an accurate sampling of the relevant dimer PES, with a significant saving of computational time. This is always a remarkable achievement, but it must be stressed that, in many cases of interest for LC modeling, FRM actually makes a fully theoretical treatment possible for systems otherwise beyond the current computational capabilities. This is of apparent importance when the goal is the reproduction of the bulk phase behavior of a well defined chemical system, for it requires an accurate description of the relevant interactions. The same information would be even more important for predicting properties that are hardly amenable to measurements, or that of unexplored materials. At the same time, it may also be useful to parameterize coarse-grained models, when the interest focuses mainly on general trends and larger systems have to be simulated for longer times.

Of course, all the above would be meaningless without a reliable test of the accuracy of FRM reconstructed potentials. We carefully checked this issue, by comparing FRM results with directly computed *ab initio* interaction energies for a variety of systems, such as biphenyl or 4-cyano-biphenyl. The quite satisfactory outcome of these tests gave us confidence that FRM potentials can be successfully employed in computer simulations.

The applications described above on liquid and solid benzene, the series of oligophenyls and that of nCB's supported our confidence. A nematic phase was predicted for *p*-quinquephenyl in the correct range of temperatures, by a simulation where each phenyl ring was modeled as an oblate Gay–Berne site with a point quadrupole. It also turned out that an accurate description of the interring torsional degree of freedom is necessary for a satisfactory reproduction of the phase diagram. The latter was also well predicted for the nCB series by atomistic simulation employing realistic potentials derived from FRM PES. In particular, we could observe a kinetically stable, orientationally ordered (nematic) phase for 5CB between 285 and 305 K, which means that transition temperatures are reproduced with a deviation of about 10 K from experimental values. The same

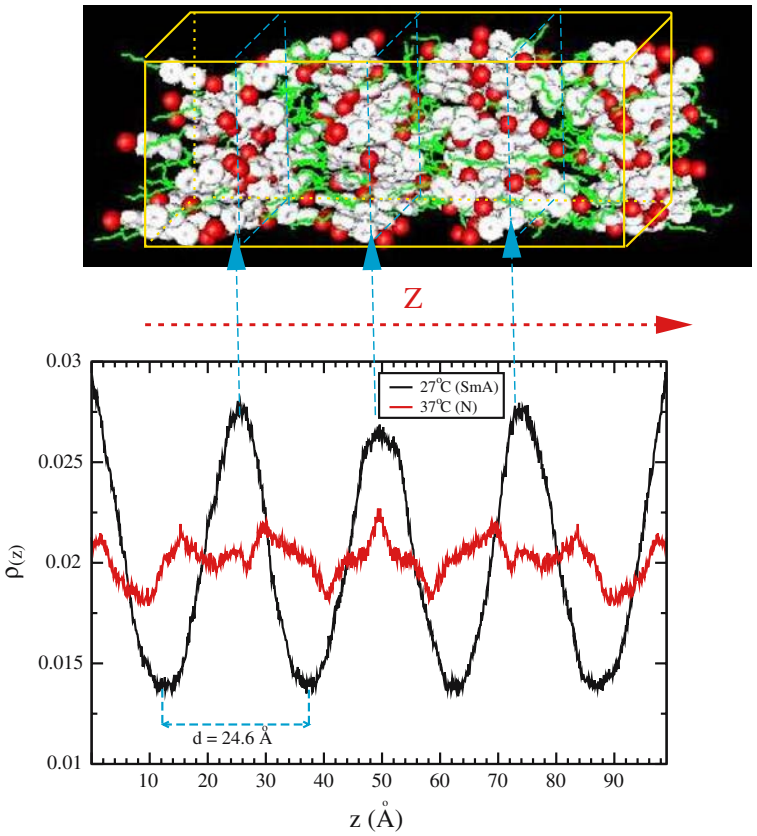

Fig. 16 8CB smectic phase. *Upper panel* a snapshot of the 8CB system at 300 K. Aliphatic chains, aromatic cores and the cyano groups have been indicated with *green*, *white* and *red colors*, respectively. *Lower panel* the number density of the same system along the normal to the smectic planes

accuracy has been achieved for 6CB and 7CB, while, in the case of 8CB, the phase diagram showed both a smectic and a nematic phase, between 300 and 310 K, and 310 and 320 K, respectively, again close to the experimental value of transition temperatures. Thus, the well known odd-even effect on transition temperatures could be accounted for remarkably well.

The transition from isotropic to nematic phase of 5CB drives significant changes in the distribution or the chain conformers, as more elongated chains are favored in the ordered phase. The connection between phase changes and conformer distribution, already found from NMR measurements, was also observed in our simulation and is presumably a key feature of the order-disorder transition for systems formed by molecules with flexible chains.

The wide range of time scales spanned by the LC dynamics is a severe challenge for simulations, especially for atomistic simulations. We found that it is necessary to carry out runs of some tens ns to obtain stable values of order parameters. This length allowed us to reach, in the case of 5CB at 290 K, a common, typically nematic, value of P_2 (0.5) starting from three different configurations at much different order parameters. It is worth stressing that this entailed a spontaneous reordering in one of these runs, from a P_2 below 0.3 to about 0.5. Despite these encouraging results, the issue of time scales is still quite severe. Some dynamic properties can reliably be calculated, noticeably so translational and rotational diffusion coefficients, while collective properties, e.g., viscosities and dielectric relaxation, are at the edge of computational modeling, particularly at lower temperatures. On the other hand, we were able to calculate the shear viscosity of the isotropic phase of 5CB with results in good agreement with the experimental data over a range of temperatures.

We can conclude that the approach employing FRM as a route to exploring the PES of dimer of complex molecules has proven successful, when tested with simulations on typical mesogenic systems as the nCB series. We are currently pursuing an extension of this approach to include, in a more systematic way, the effect of internal degrees of freedom on the calculated dimer PES, as the interplay between intra and intermolecular interactions is recognized instrumental in determining phase diagram and dynamic properties, especially in LC.

References

1. Crain J, Komolkin A (1999) Adv Chem Phys 109:39
2. Atomistic simulation and modeling of smectic liquid crystals in Advances in the Computer Simulations of Liquid Crystals NATO ASI series, edited by P. Pasini and C. Zannoni; Kluwer: Dordrecht, 2000

3. Wilson M (2005) Int Rev Phys Chem 24:421
4. Care C, Cleaver D (2005) Rep Prog Phys 68:2665
5. Collings P (1990) Liquid crystals—nature's delicate phase of matter. Adam Hilger: Bristol
6. deGennes P, Prost J (1993) The Physics of Liquid Crystals, 2nd edn. Oxford University Press, Oxford
7. Brooks BR, Bruccoeri RE, Olafson BD, States DJ, Swaminanthan S, Karplus M (1983) J Comp Chem 4:187
8. Hermans J, Berendsen H, van Gusteren W, Postma J (1984) Biopolymers 23:1
9. Wiener SJ, Kollmann PA, Nguyen DT, Case DA (1986) J Comp Chem 7:230
10. Jorgensen W, Severance D (1990) J Am Chem Soc 112:4768
11. Car R, Parrinello M (1985) Phys Rev Lett 55:2471
12. Marx D, Hutter J (2000) Ab Initio molecular dynamics: theory and implementation in modern methods of quantum chemistry; NIC series, Vol I: Forshungszentrum, Jülich, D,
13. Amovilli C, Cacelli I, Campanile S, Prampolini G (2002) J Chem Phys 117:3003
14. Bizzarri M, Cacelli I, Prampolini G, Tani A (2004) J Phys Chem A 108:10336
15. Cacelli I, Cinacchi G, Prampolini G, Tani A Computer simulation of mesogen with ab initio interaction potentials in novel approaches to the Structure and Dynamics of Liquids. Experiments, Theories and Simulation edited by J. Samios and V. Durov; Kluwer: Dordrecht, 2004
16. Cacelli I, Prampolini G, Tani A (2005) J Phys Chem B 109:3531
17. Karlström G, Linse P, Wallqvist A, Jönsson B (1983) J Am Chem Soc 105:3777
18. Linse P (1984) J Am Chem Soc 106:5425
19. Linse P, Engström S, Jönsson B (1985) Chem Phys Lett 115:95
20. Corongiu G, Migliore M, Clementi E (1989) J Chem Phys 90:4629
21. Millot C, Stone A (1992) Mol Phys 77:439
22. Soetens J, Millot C (1995) Chem Phys Lett 235:22
23. Liu Y, Kim K, Berne B, Friesner R, Rick S (1998) J Chem Phys 108:4739
24. Allen MP, Evans GT, Frenkel D, Mulder B (1993) Adv Chem Phys 86:1
25. Zannoni C (2001) J Mater Chem 11:2637
26. Cacelli I, Cinacchi G, Geloni C, Prampolini G, Tani A (2003) Mol Cry Liq Cry 395:171
27. Fukunaga H, Takimoto J, Aoyagi T, Shoji T, Sawa F, Doi M (2001) Mol Cry Liq Cry 365:1695
28. Prampolini G (2006) J Chem Theory Comput 2:556
29. Cacelli I, Cinacchi G, Prampolini G, Tani A (2004) J Chem Phys 120:3648
30. Cacelli I, Cinacchi G, Prampolini G, Tani A (2004) J Am Chem Soc 126:14278
31. De Gaetani L, Prampolini G, Tani A (2006) J Phys Chem B 110:2847
32. Cacelli I, De Gaetani L, Prampolini G, Tani A Mol Cry Liq Cry (in press)
33. Cacelli I, De Gaetani L, Prampolini G, Tani A (2007) J Phys Chem B (in press)
34. Shi X, Bartell L (1988) J Phys Chem 92:5667
35. Claessens M, Ferrario M, Ryckaert (1983) J Mol Phys 50:217
36. Jaffe RL, Smith GD (1996) J Chem Phys 105:2780
37. Hobza P, Selzle HL, Schlag EW (1996) J Phys Chem 100:18790
38. Cabaço M, Danten Y, Besnard M, Guissani Y, Guillot B (1997) J Phys Chem B 101:6977
39. Chelli R, Cardini G, Procacci P, Righini R, Califano S (2000) J Chem Phys 113:6851
40. Tsuzuki S, Honda K, Uchimaru T, Mikami M, Tanabe K (2002) J Am Chem Soc 124:104
41. Witt R, Sturz L, Dölle A, Müller-Plathe F (2000) J Phys Chem A 104:5716
42. Picken SJ, VanGunsteren WF, VanDujen PT, DeJeu WH (1989) Liq Cryst 6:357
43. Komolkin AV, Laaksonen A, Maliniak A (1994) J Chem Phys 101:4103
44. Clark SJ, Adam CJ, Cleaver DJ, Crain J (1997) Liq Cryst 22:477
45. Stevensson B, Komolkin A, Sandström D, Maliniak A (2001) J Chem Phys 114:2332
46. Adam C, Clark S, Wilson M, Ackland G, Crain J (1998) Mol Phys 93:947
47. Zakharov A, Komolkin AV, Maliniak A (1999) Phys Rev E 59:6802
48. Zakharov A, Maliniak A (2001) Eur Phys J E 4:435
49. Cheung LD, Clark S, Wilson M (2002) Chem Phys Lett 356:140
50. Glaser MA (2000) Atomistic simulation and modeling of smectic liquid crystals in Advances in the Computer Simulations of Liquid Crystals NATO ASI series, edited by P. Pasini and C. Zannoni; Kluwer: Dordrecht
51. Lansac Y, Glaser M, Clark N, Lavrentovich O (1999) Nature 398:54
52. Lansac Y, Glaser M, Clark N (2001) Phys Rev E 64:051703
53. Emsley J, Luckhurst G, Stockley C (1981) Mol Phys 44:565
54. Dvinskikh SV, Furò I (2001) J Chem Phys 115:1946
55. Hanemann T, Haase W, Svodoba I, Fuess H (1995) Liq Cryst 19:699
56. Adam C, Ferrarini A, Wilson M, Ackland G, Crain J (1999) Mol Phys 97:541
57. Sandmann M, Hamann F, Wurflinger A (1997) Z Naturforsh 52:739
58. Oweimreen G, Morsy M (2000) Thermochimica Acta 346:37
59. Dong R (1998) Phys Rev E 57:4316
60. Watanabe H, Sato T, Hirose M, Osaki K, Yao M (1998) Rheologica Acta 37:519
61. Jadzin J, Czechowsky G (2003) Phys Rev E 67:041705
62. Li J, Wang I, Fayer M (2005) J Phys Chem B 109:6514
63. Jadzin J, Lech RDT, Czechowski G (2001) J Chem Eng Data 46:110
64. Seo DS, Matsuda H, Ide TO, Kobayashi S (1993) Mol Cry Liq Cry 224:13
65. Blinov LM, Cipparone RBC, Iovane M, Checco A, Lazarev VV, Palto SP (1999) Liq Cryst 26:427
66. Claverie P (1978) Elaboration of approximate formulas for the interaction between large molecules: application in organic chemistry, In: Pullmann B, Intermolecular–Interaction: from diatomics to biopolymers, Wiley, London
67. Zhang D, Zhang J (2003) J Chem Phys 119:3599
68. Gay JG, Berne B (1981) J Chem Phys 74:3316
69. Cleaver DJ, Care CM, Allen MP, Neal NP (1996) Phys Rev E 54:559
70. Buckingam A (1978) Adv Chem Phys 12:107
71. Amovilli C, March NH (2005) Carbon 43:1634
72. Boys SF, Bernardi F (1970) Mol Phys 19:553
73. Tsuzuki S, Uchimaru T, Mikami M, Tanabe K (1996) Chem Phys Lett 252:206
74. Becke A (1993) J Chem Phys 98:5648
75. Frisch MJ et al. (2003) Gaussian 03 (Revision A.1). Gaussian Inc., Pittsburgh
76. Metropolis N, Rosenbluth AW, Rosenbluth MH, Teller AH, Teller E (1953) J Chem Phys 21:1087
77. Paschen D, Geiger A (2000) MOSCITO 3.9; Department of Physical Chemistry: University of Dortmund

78. Berendsen HJC, Postma JPM, van Gusteren WF, Di Nola A, Haak JR (1984) J Chem Phys 81:3684
79. Ryckaert JP, Ciccotti G, Berendsen HJC (1977) J Comput Phys 55:3336
80. Darden T, York D, Pedersen L (1993) J Chem Phys 98:10089
81. Essmann U, Perera L, Berkowitz M, Darden A, Lee H, Pedersen L (1995) J Chem Phys 103:8577
82. Allen M, Tildesley D (1987) Computer simulation of liquids. Oxford, Clarendon
83. Dymond J, Smith E (1969) The virial coeficients of gases: a critical compilation. Clarendon Press, Oxford
84. Handbook of chemistry and physicis CRC press, Boca Raton, 1997
85. Bacon G, Curry N, Wilson S (1964) Proc Roy Soc Lond A 279:98
86. Timmermans J (1950) Physical chemical constants of pure organic compounds. Elsevier, Amsterdam
87. Smith G (1979) Mol Cry Liq Cry 49:207
88. Klüner, R (1995) Rotatorische Dynamik von Kohlenwasserstoffen in flüssiger Phase; Shaker-Verlag, Aachen
89. Grolier J, Roux-Desgranges G, Berkane M, Jimenez E, Wilhelm E (1993) J Chem Thermodynam 25:41
90. Majer V, Svoboda V (1985) Enthalpies of vaporization of organic compounds: a critical review and data compilation. Blackwell, Oxford
91. Falcone D, Douglass D, McCall D (1967) J Phys Chem 71:2754
92. Landolt-Börnstein (1969) Zahlenwerte und Funktionen, Band II, Teil 5, Transport Phänomene; Springer, Berlin Heidelberg New York
93. Linde B, Lezhnev N (2000) Ultrasonics 38:945
94. Cacelli I, Prampolini G (2003) J Phys Chem A 107:8665
95. Smit G (1977) Mol Cry Liq Cry 49:207
96. Irvine PA, Wu C, Flory P (1984) J Chem Soc Faraday Trans 80:1795
97. Bastiansen O, Fernholt L, Cyvin BCS, Samdal S, Almenningen A (1985) J Mol Struct 128:59
98. Bastiansen O, Samdal S (1985) J Mol Struct 128:115
99. Steele D, Eaton V (1973) J Chem Soc Faraday Trans 69:1601
100. Delugeard Y, Charbonneau G (1976) Acta Crystallogr B 33:1586
101. Baker K, Fratini A, Resch T, Knachel H, Adams W, Socci E, Farmer B (1993) Polym Pap 69:1601
102. Hautpmann S, Mosell T, Reiling S, Brickmann J (1996) J Chem Phys 208:57
103. Dvinskikh S, Furo' I (2001) J Chem Phys 115:1946
104. Calucci L, Geppi M (2001) J Chem Inf Comput Sci 41:1006
105. Catalano D, Cifelli M, Geppi M, Veracini C (2001) J Phys Chem A 105:34
106. Dong R (1988) J Chem Phys 88:3962
107. Dong R, Richards G (1992) Chem Phys Lett 200:541
108. Deeg F, Greenfield S, Stankus J, Newell V, Fayer M (1990) J Chem Phys 93:3503
109. Gottke SD, Cang H, Bagchi B, Fayer M (2002) J Chem Phys 116:6339
110. Béguin A, Billard J, Bonamy F, Buisine J, Cuivalier P, Dubois J, Barny PL (1984) Mol Cry Liq Cry 115:119
111. Ferrarini A, Luckhurst G, Nordio L (1995) Mol Phys 85:131
112. Ojha D, Kumar D, Pisipati V (2002) Cryst Res Technol 37:881
113. Berardi R, Muccioli L, Zannoni C (2004) Chem Phys Chem 5:104